ARL-TR-2551
AD

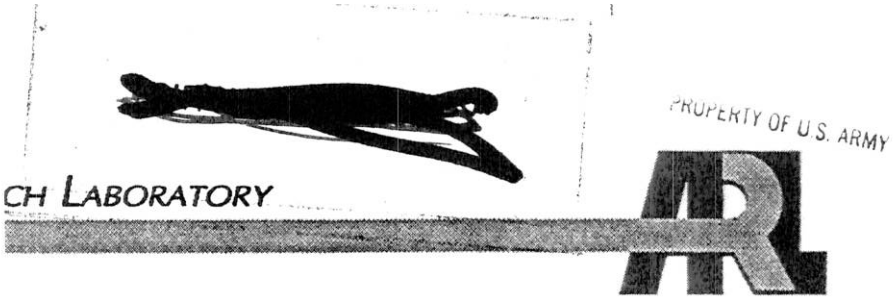

Burning Phenomena of Solid Propellants

by Martin S. Miller and John A. Vanderhoff

ARL-TR-2551 July 2001

Abstract

Dynamic behavior of the burning surface of propellants has been captured as a function of pressure via movies taken with a 30-frames/s video camera. These movies can be played with the CD version of this manuscript. A windowed vessel capable of pressurization was used to burn the propellants XM39, M43, HMX2, M10, M30, JA2, and RDX over a pressure range from 0.1 to 3 MPa. The SVHS video camera was angled down to capture the dynamic surface behavior and provide some basis for assessing the validity of a one-dimensional approximation of the surface. Along with these propellant movies, plots of linear burning rate vs. pressure have been included.

Contents

List of Figures v

List of Tables vii

1. Introduction 1

2. Background 1

3. Experiment 2

4. Results 5

5. Summary 6

6. References 15

Appendix 19

Distribution List 21

Report Documentation Page 23

INTENTIONALLY LEFT BLANK.

List of Figures

Figure 1. The top diagram (a) is a sketch of the windowed strand burner system and the associated components used to capture propellant burning on video. The bottom left photo (b) shows the windowed strand burner, and the bottom right photo (c) shows the remote control and acquisition electronics 3

Figure 2. XM39 propellant combustion at pressures from 0.7 to 3.0 MPa. 7

Figure 3. M43 propellant combustion at pressures from 0.7 to 3.0 MPa 8

Figure 4. XM39 burning at 3.0 MPa 9

Figure 5. M43 burning at 0.4 MPa. 9

Figure 6. HMX2 propellant combustion at pressures from 1.0 to 3.0 MPa. 9

Figure 7. M10 burning at 2.0 MPa. 10

Figure 8. M30 burning at 0.5 MPa. 10

Figure 9. JA2 burning at 1.5 MPa. 10

Figure 10. RDX burning at 1.5 MPa. 10

Figure 11. Burning rate of M43 vs. pressure. The pressurizing gas was N_2 11

Figure 12. Burning rate of XM39 vs. pressure. The pressurizing gas was N_2 11

Figure 13. Burning rate of HMX2 vs. pressure. The pressurizing gas was N_2 12

Figure 14. Burning rate of M10 vs. pressure. The pressurizing gas was N_2 12

Figure 15. Burning rate of M30 vs. pressure. The pressurizing gas was N_2 13

Figure 16. Burning rate of JA2 vs. pressure. 13

Figure 17. Burning rate of RDX as a function of pressure. 14

INTENTIONALLY LEFT BLANK.

List of Tables

Table A-1. Some properties of the propellants shown in the video movies. 19

Table A-2. Burn rate data fitted to $r=Ap^n$, where r is the burn rate in cm/s and p is the pressure in MPa. 20

Burning Phenomena of Solid Propellants

by

Martin Miller and John Vanderhoff

1. Introduction

Over the last 15 years in the Ignition and Combustion Branch of the Ballistic Research Laboratory (BRL), Aberdeen Proving Ground, MD, more recently re-organized as the Army Research Laboratory (ARL), we have been performing combustion-diagnostic experiments on burning propellants. These experiments included measuring the burn rate as a function of pressure, measuring the temperature and species concentration profiles and observing propellant burning surface phenomena as a function of pressure and propellant type. For many of these measurements, a video camera recorded the propellant burn on VHS or SVHS tape. Occasionally, single frames were used in manuscripts to emphasize some feature of the propellant burn; however, no movies of these propellant burns were ever published. We believe there is unique information contained in these video movies; thus, prior to the author's (John Vanderhoff) retirement, these data are herein documented.

Visual records for three classes of energetic materials are presented: homogeneous propellants (M10, JA2 and M30), composite propellants (XM39, M43 and HMX2), and a major energetic crystalline component (RDX). These propellant compositions and other characteristics are given in Table A-1 of Appendix A. Except for RDX and M30, these propellants exhibit a distinct dark zone (no visible illumination) where the gas phase temperature plateaus about halfway between ambient temperature and the final flame temperature. A variety of burning behavior is demonstrated in these movies—melting, ebullition, hot spots, flaking, and floating carbonaceous particles are dynamically represented. Hence, future efforts to include surface phenomena in detailed combustion models could benefit from these video observations.

While the propellant burning movies comprise the majority of this manuscript, burning rates as a function of pressure (many not published before) are also included here.

2. Background

According to Strehlow (1984),

> "The burning zone of a solid propellant is somewhat more complex than the equivalent region in a premixed flame. Furthermore, even though it is customary to discuss a one-dimensional solid-propellant combustion wave, it is doubtful if one can ever hope to observe strictly one-dimensional combustion during the burning of a solid-propellant grain.

> The inherent three-dimensional structure that appears in the burning zone of a solid-propellant does not arise from the type of transverse instability which leads to non-one-dimensional detonation fronts but mainly appears because of inhomogeneities in the structure of the propellant grain itself. It is observed that the burning roughness or lack of one-dimensionality becomes more severe as one changes from a simple extruded double-base to a composite propellant."

Nonetheless, models of propellant combustion are usually modeled as a one-dimensional process, where the action coordinate is normal to the burning surface. The simplest approximation of the burning surface is a discontinuity between condensed and gas phases, such as in the model of Rice and Ginnell (1950). Models more involved with the surface region modify this boundary by considering some form of porosity factor to describe a finite region between the solid and gas phases, but still retain the one-dimension assumption. Models by Parr and Crawford (1950), Maksimov and Merzhanov (1966), Hatch (1986), and Kuo and Ling (1994) feature this type of approach. We do not know of any published work where the mathematical formulation of the solid propellant combustion model is multidimensional.

3. Experiment

A diagram of the windowed strand burner and pertinent circuitry is shown in Figure 1(a). The chamber is stainless steel with a rectangular outside shape (5 in x 5 in x 8 in). The interior shape is a right circular cylinder of 3 in diameter, where four opposed cutouts provide rectangular clear aperture optical access of .75 in x 3 in. One side of the windowed strand burner, with details of the window mounting and optical access, is shown photographically in Figure 1(b). In determining propellant burn rates, the video camera is oriented normal to the burning strand, as shown in Figure 1(b), except that a mirror is used to turn the image 90° to protect the camera in case of window failure. This configuration does not allow a view of the burning surface; thus, in this report (except for the RDX movie), the camera was operated in an elevated position, as shown in Figure 1(a). A strobe lamp provides backlighting for most of the propellant movies. These movies were taken at a framing rate of 30/s and stored on SVHS or VHS tape. Two different methods are available for maintaining a constant pressure during the course of a propellant burning experiment. The primary method maintains nitrogen flow around the propellant sample by inserting a critical orifice in the opened exhaust line. This orifice allows nitrogen gas flow which is greater than the flow generated by combustion gases. The nitrogen bank regulator maintains a set pressure. Alternatively, a constant-pressure no-flow situation can be achieved by closing the exhaust line and opening the

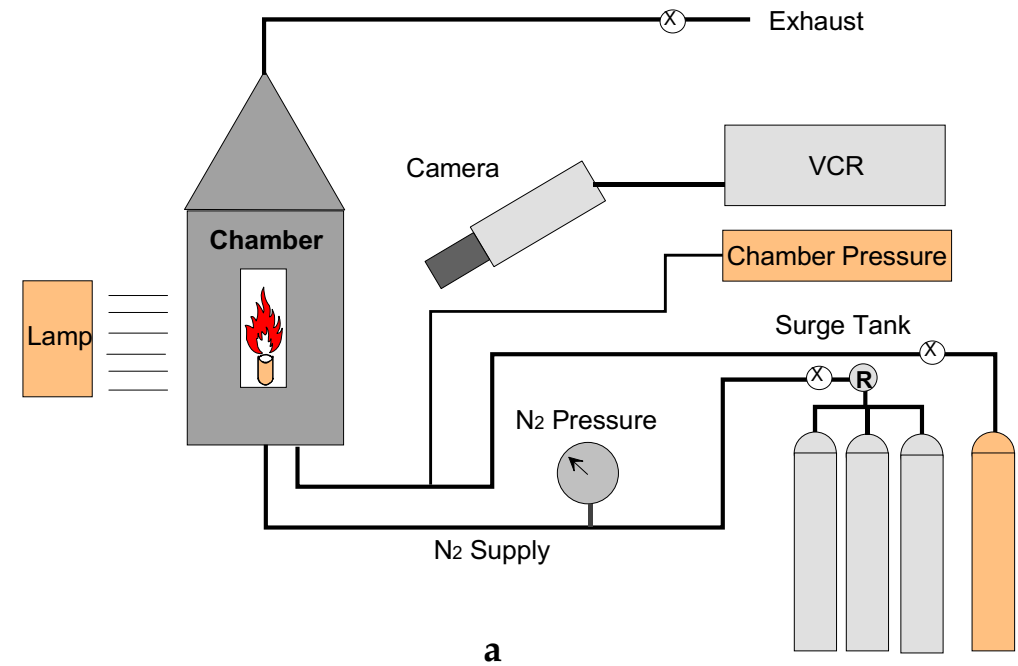

a

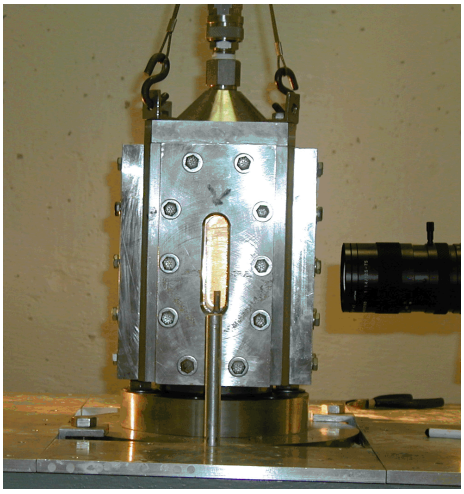

b

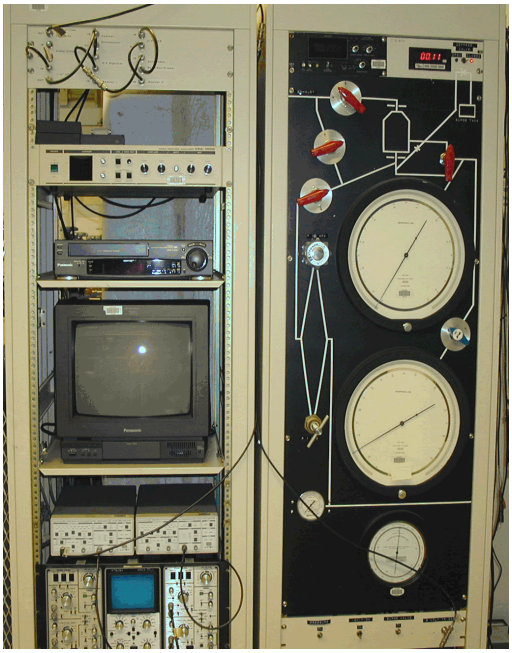

c

Figure 1. The top diagram (a) is a sketch of the windowed strand burner system and the associated components used to capture propellant burning on video. The bottom left photo (b) shows the windowed strand burner, and the bottom right photo (c) shows the remote control and acquisition electronics.

surge tank line. Here, the total volume of the windowed strand burner chamber (0.9 liters) and the surge tank (50 liters) are sufficiently large that gas generated by combustion adds negligibly to the pressure. The strand burner can operate over a pressure range from a rough vacuum to 10 MPa. As a safety precaution, the strand burner is operated in a small room with reinforced concrete walls. Pressurized operations are conducted remotely, and some of the controls and data acquisition equipment can be seen in Figure 1(c). Pressure readout devices, control knobs, and control valves are contained in the instrument rack on the right. The data acquisition instruments are housed in the left rack.

After pressurization and activation of the data acquisition and control electronics, the experiment commences with the hot wire ignition of the propellant sample. A length of 30 gauge nickel wire is kinked in the center and glued into a small hole drilled in the top center of the propellant sample (propellant sample diameters are given in Appendix A, Table A-1). Part of the ignition process is captured in the video movies; thus, the geometry of the wire placement is clearly identified. Combustion proceeds from the top center of the sample, creating a bowl-like combustion surface. This bowl tends to flatten as combustion proceeds, and the quality of the video movie decreases due to an accumulation of smoke in the video path. The bowl created by the point heating of wire ignition prevented side burning of the samples in the following way. In many cases, melting occurs in the center portions of the combustion surface but the cooling effects at the edges keep the flaming liquid from running over the side. At high pressure, edge cooling is not sufficient to prevent side burning. For these cases, the experimenter must resort to coating the sample sides with an inhibitor.

One set of experiments (RDX combustion) incorporated a different strand burner and a CO_2 laser for ignition (see Homan and Vanderhoff [1999] for details). For this work, it was crucial to create a planar burning surface. This was accomplished by ignition with a uniform laser beam of diameter similar to the propellant sample.

As previously mentioned, the burning rates reported herein were obtained with the camera angle normal to the burning strand. With this orientation little of the surface phenomenology can be observed. Consequently, with the exception of the RDX movie, all the movies in this report have the camera angled down at the surface with enough magnification to see many details of the burning surface for many propellants. These video tape data were much later digitized with a miroVIDEO DC30 board and captured using Adobe Premiere 4.2 software. A frame size of 320 x 240 and a framing rate of 15 frames/s were selected. Two different compressions (codecs) were employed so that the majority of PC users can view the movies without installing additional software.

The files with the .avi extension have been made using the Intel Indeo video 5.04 [32] codec and can be played with Windows Media Player. Only one movie can

be displayed at a time, and the mouse can be used to drag to any individual frame. The files with the .mov extension have been made using the Cinepak codec by Radius [32] and can be played with the QuickTime Player. Here, multiple movies can be played simultaneously, and the arrow keys can be used to move through the movie frame by frame.

4. Results

Figures 2–10 are video frames of propellant combustion at a given pressure. The complete movie can be run by clicking on the hyperlink contained in the caption. Most extensively documented are two low vulnerability nitramine propellants, XM39 and M43. For both of these propellants, a mobile black particulate appears on the surface. Movement of these black particulates is probably occurring on a thin liquid layer. These observations are consistent with earlier work reporting the presence of carbonized fragments during the combustion of nitramine propellants, work by Zimmer-Galler (1968) and Parr and Hanson-Parr (1995). Both XM39 and M43 have a substantial part of the burning surface covered with the black particulate at the lowest pressures (0.4 to 0.7 MPa). As the pressure increases, the amount of covering decreases. However, for M43, the surface again becomes largely covered in the 1.5–2.0 MPa pressure range. This M43 particulate re-covering corresponds to the same pressure range where an anomaly (a bump) occurs in the linear burning rate versus pressure curve.

As mentioned earlier, most of the propellants investigated here exhibit a distinct dark zone region in the pressure regime studied; in fact, for some of the lowest pressures investigated, a visible flame is not established. In general, more energetic propellants manifest visible flames at lower pressures. RDX burns with a visible flame at atmospheric pressure, and of the propellants studied, M43 has the lowest pressure visible flame, ~ 0.7 MPa. M10 and JA2 develop a visible flame around 1 MPa, and both of these propellants burn with small surface flamelets. XM39 and HMX2 develop visible flames around 1.5 MPa and have similar burn rates. Dynamically, the burning surface of HMX2 appears much more bubbly than does XM39. These dynamic differences could be a function of binder characteristics. M30 is the only propellant studied here where a visible flame is established and attached to the surface for the entire pressure range studied (i.e., no dark zone). One can observe the flaking off of a disk of particulate matter during the course of the 0.5 MPa burn. M30 has a crystalline component, nitroguanidine, as the major component, and it has been speculated that decomposition of this component will contain substantial amounts of NH_x species. Moreover, finite rate chemistry studies demonstrate that the dark zone shrinks with increasing NH_x species, giving a plausible explanation for not

observing a dark zone in M30. For a more complete discussion of this proposed kinetic mechanism, see Miller and Anderson (2000).

The description (interpretation) of characteristics of the propellant burning is kept brief here so as not to bias the reader, but rather to promote reader impressions derived from viewing and comparing the propellant movies.

Figures 11–17 are plots of linear burning rate versus pressure for the various propellants studied here. These various data are fitted to the standard equation $r = Ap^n$, and the values for A and n are given in Appendix A, Table A-2. Here, r is the burn rate in cm/s and p is the pressure in MPa. There is quite a range of values for A and n, depending on the pressure range over which the fitting was obtained. Perhaps the most inappropriate use of this equation is for M43, where a significant bump in the burn rate occurs.

5. Summary

The goal of this report is to document a variety of propellant combustion properties and provide the reader with a look at the dynamic processes occurring on the surface of a combusting propellant. One-dimensional combustion models have been used to predict and/or verify experimental phenomena for many years. It is hoped that this report provides some basis for assessing the validity of that approximation.

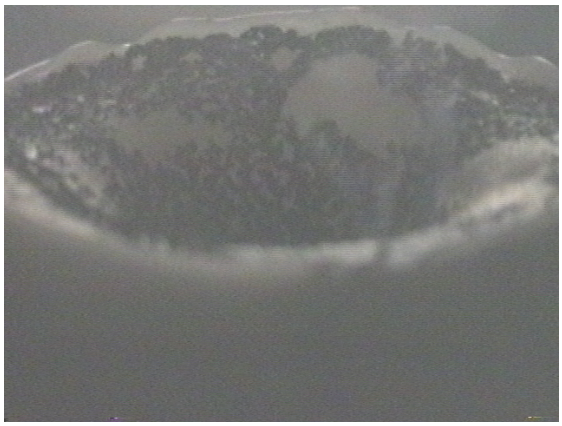

a. XM39 burning at 0.7 MPa.
xm39\xm397m.avi xm39\xm397m.mov

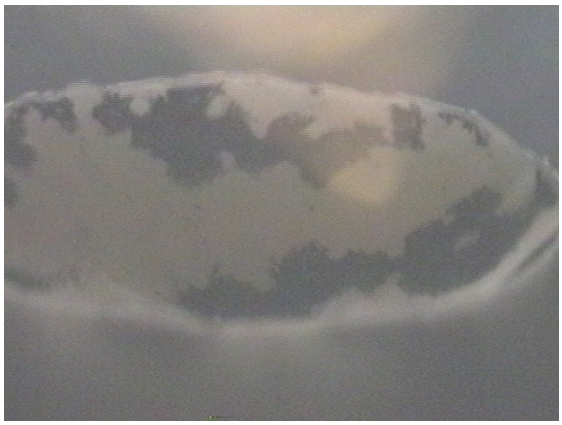

d. XM39 burning at 1.5 MPa.
xm39\xm3915m.avi xm39\xm3915m.mov

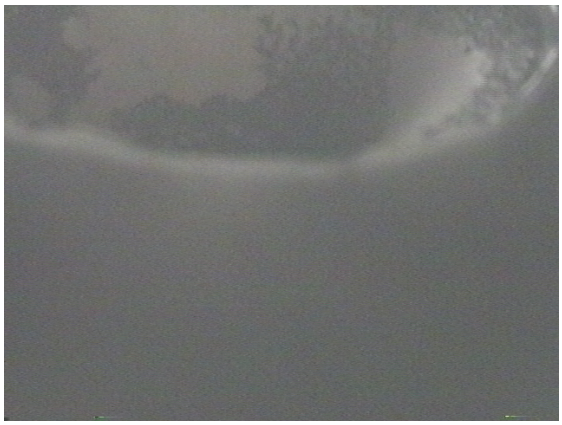

b. XM39 burning at 1.0 MPa.
xm39\xm3910m.avi xm39\xm3910m.mov

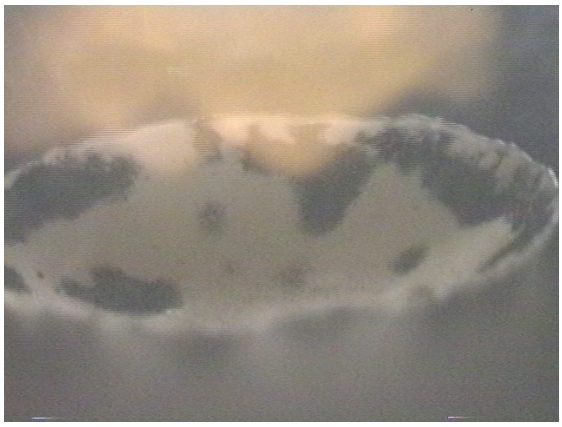

e. XM39 burning at 2.0 MPa.
xm39\xm3920m.avi xm39\xm3920m.mov

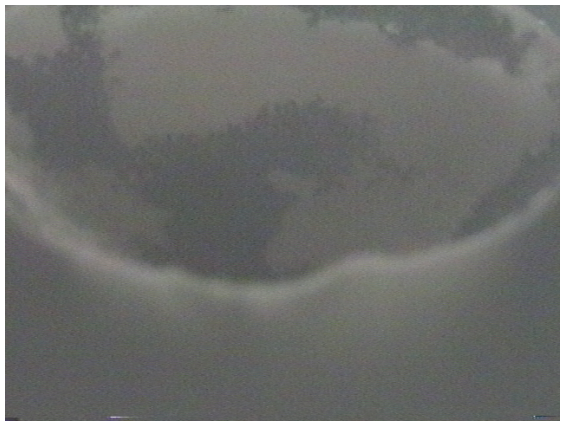

c. XM39 burning at 1.2 MPa.
xm39\xm3912m.avi xm39\xm3912m.mov

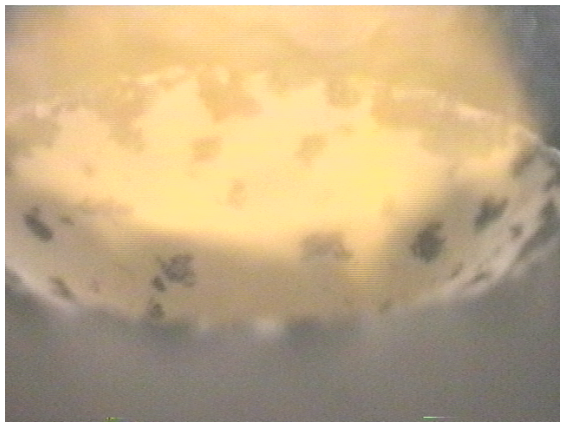

f. XM39 burning at 3.0 MPa.
xm39\xm3930m.avi xm39\xm3930m.mov

Figure 2. XM39 propellant combustion at pressures from 0.7 to 3.0 MPa.

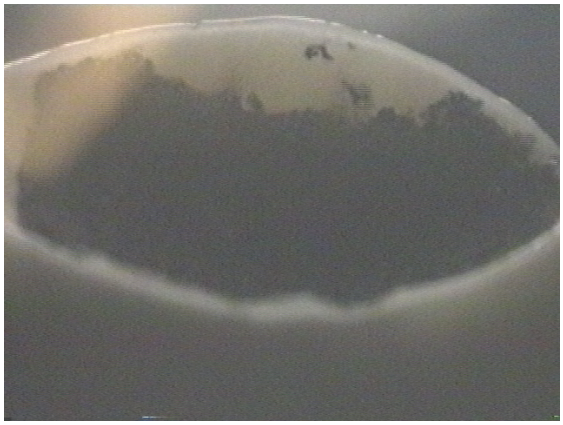

a. M43 burning at 0.7 MPa.
m43\m437m.avi m43\m437m.mov

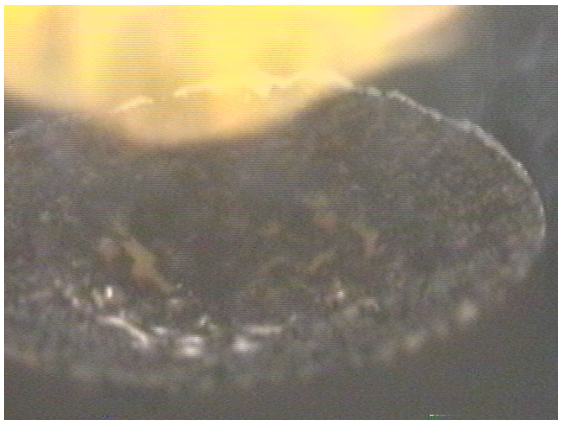

d. M43 burning at 1.5 MPa.
m43\m4315m.avi m43\m4315m.mov

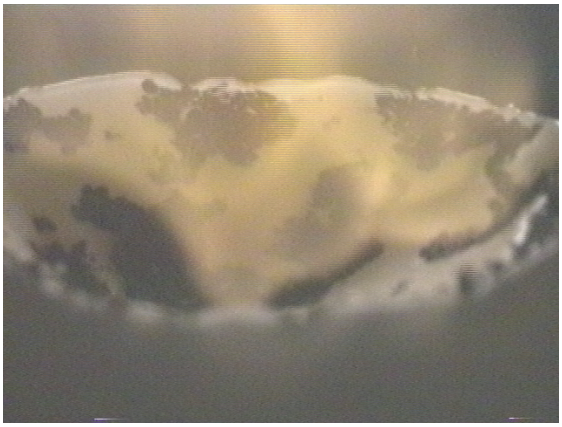

b. M43 burning at 1.0 MPa.
m43\m4310m.avi m43\m4310m.mov

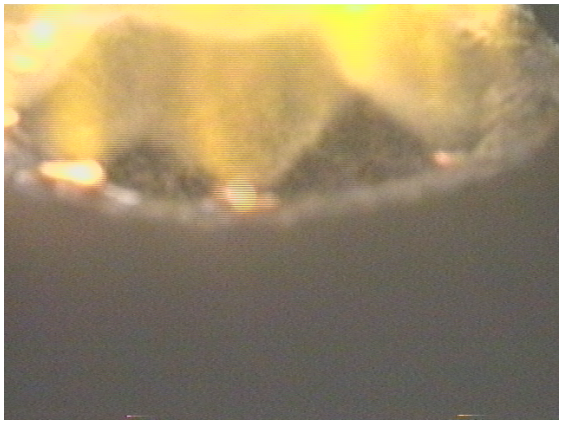

e. M43 burning at 2.0 MPa.
m43\m4320m.avi m43\m4320m.mov

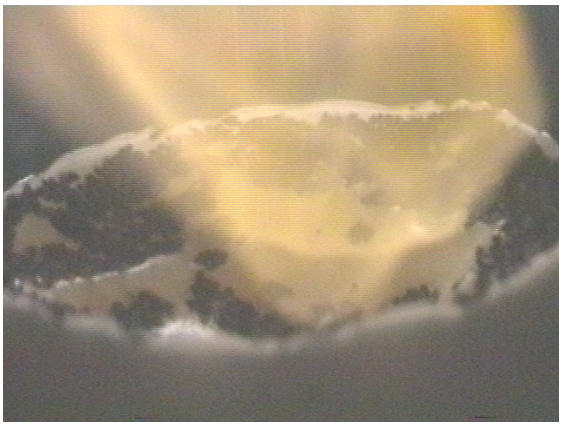

c. M43 burning at 1.2 MPa.
m43\m4312m.avi m43\m4312m.mov

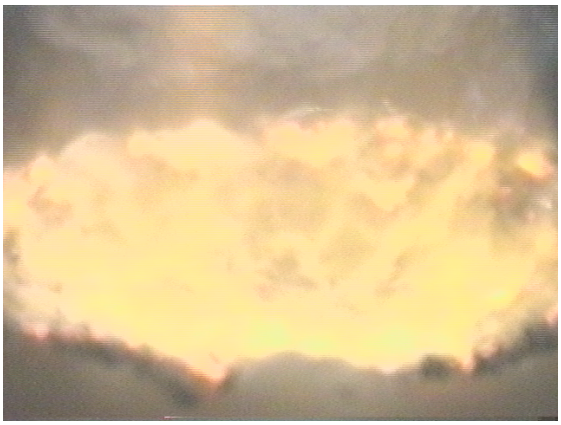

f. M43 burning at 3.0 MPa.
m43\m4330m.avi m43\m4330m.mov

Figure 3. M43 propellant combustion at pressures from 0.7 to 3.0 MPa

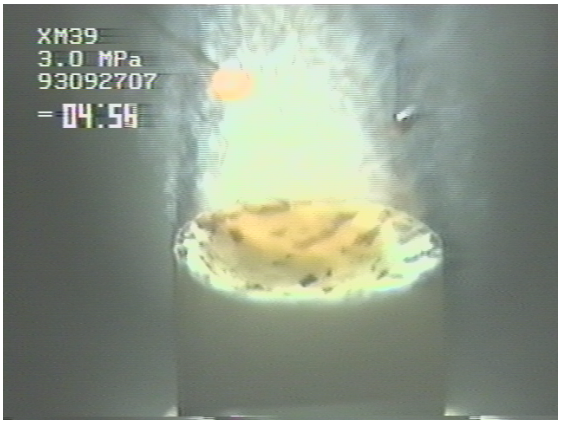

Figure 4. XM39 burning at 3.0 MPa
xm39\xm39bm.avi xm39\xm39bm.mov

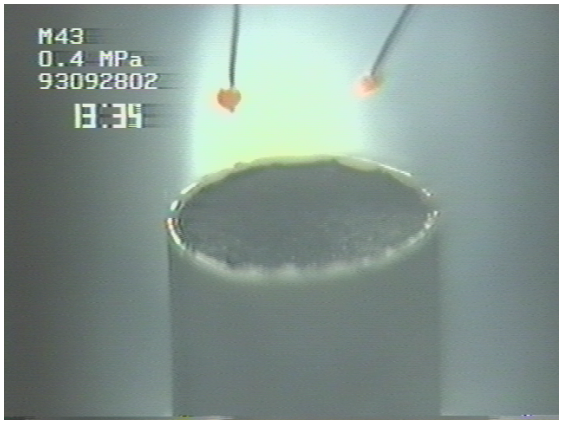

Figure 5. M43 burning at 0.4 MPa.
m43\m43bm.avi m43\m43bm.mov

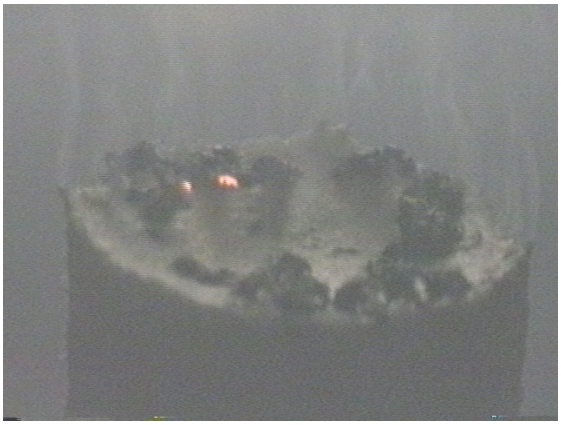

a. HMX2 burning at 1.0 MPa.
hmx2\hmx210m.avi hmx2\hmx210m.mov

c. HMX2 burning at 2.0 MPa.
hmx2\hmx220m.avi hmx2\hmx220m.mov

b. HMX2 burning at 1.5 MPa.
hmx2\hmx215m.avi hmx2\hmx215m.mov

d. HMX2 burning at 3.0 MPa.
hmx2\hmx230m.avi hmx2\hmx230m.mov

Figure 6. HMX2 propellant combustion at pressures from 1.0 to 3.0 MPa.

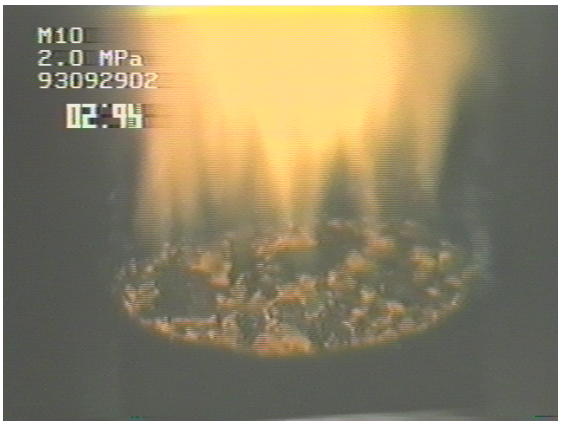

Figure 7. M10 burning at 2.0 MPa.
m10\m10m.avi m10\m10m.mov

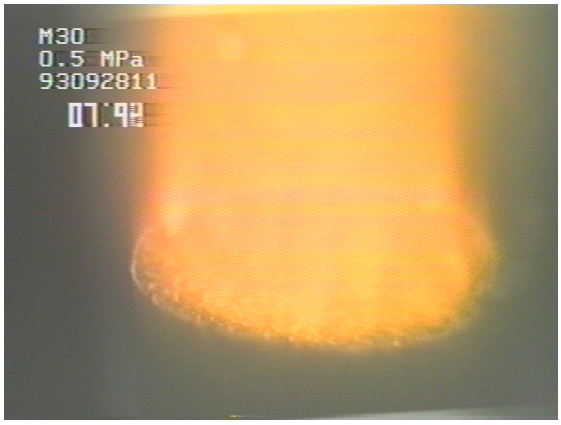

Figure 8. M30 burning at 0.5 MPa.
m30\m30m.avi m30\m30m.mov

Figure 9. JA2 burning at 1.5 MPa.
ja2\ja2m.avi ja2\ja2m.mov

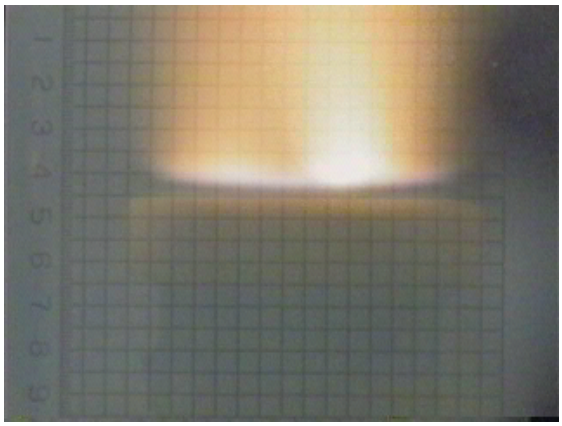

Figure 10. RDX burning at 1.5 MPa.
rdx\rdxmovie.avi

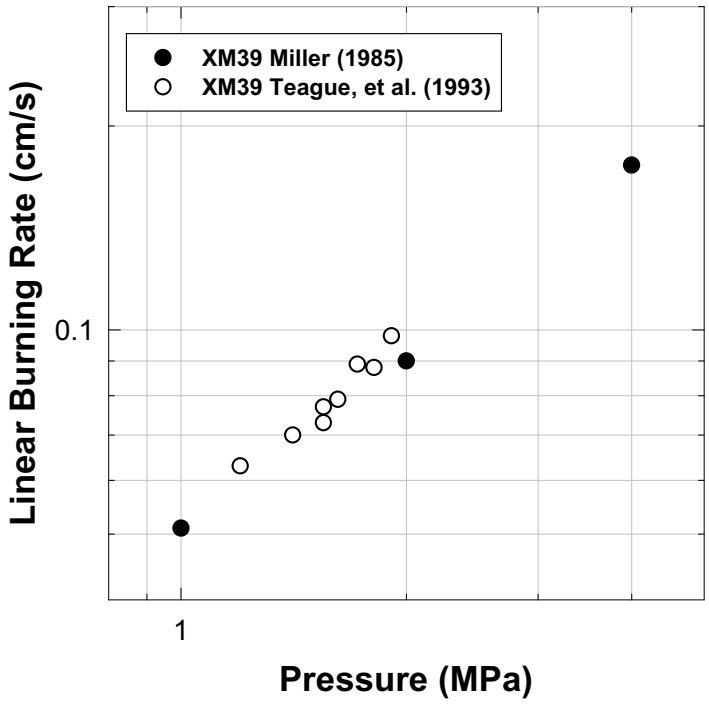

Figure 11. Burning rate of M43 vs. pressure. The pressurizing gas was N_2.

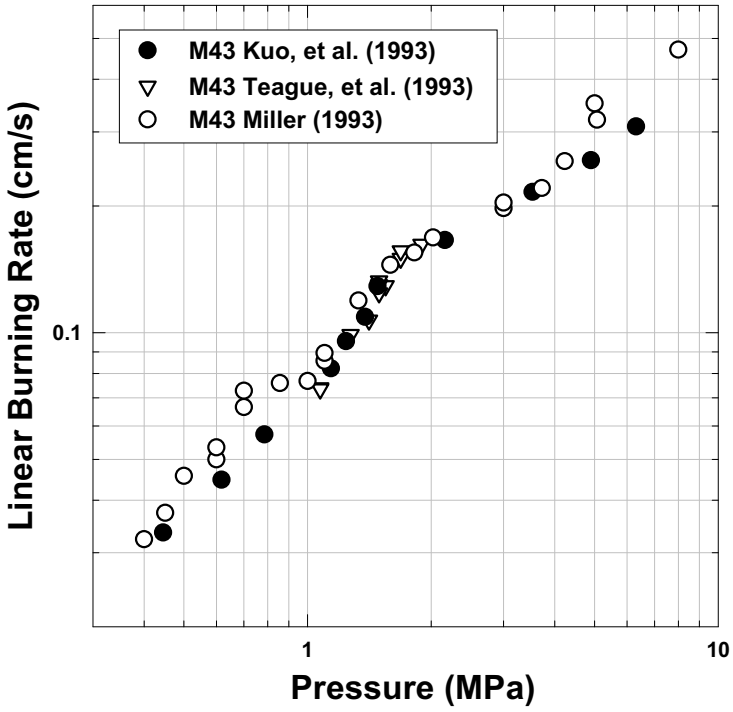

Figure 12. Burning rate of XM39 vs. pressure. The pressurizing gas was N_2.

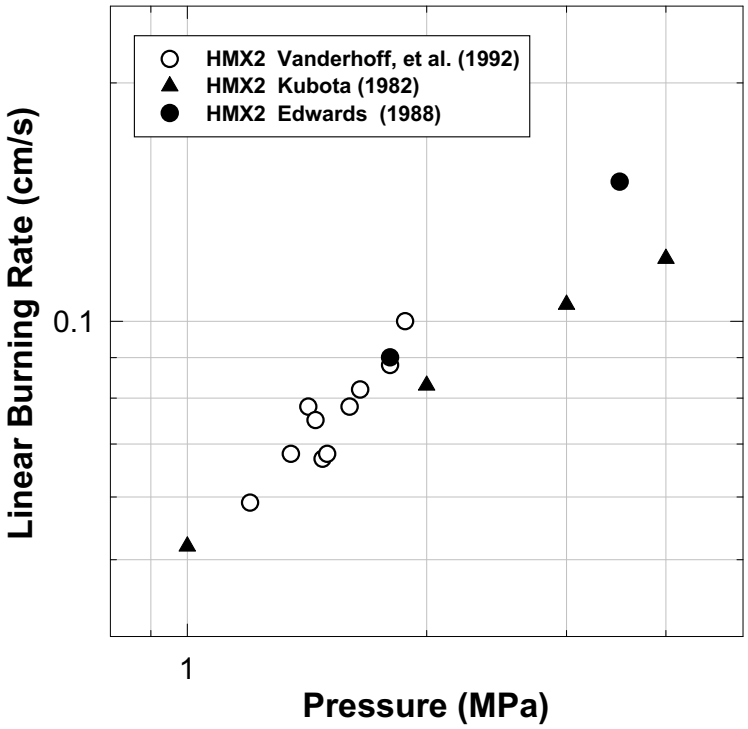

Figure 13. Burning rate of HMX2 vs. pressure. The pressurizing gas was N_2.

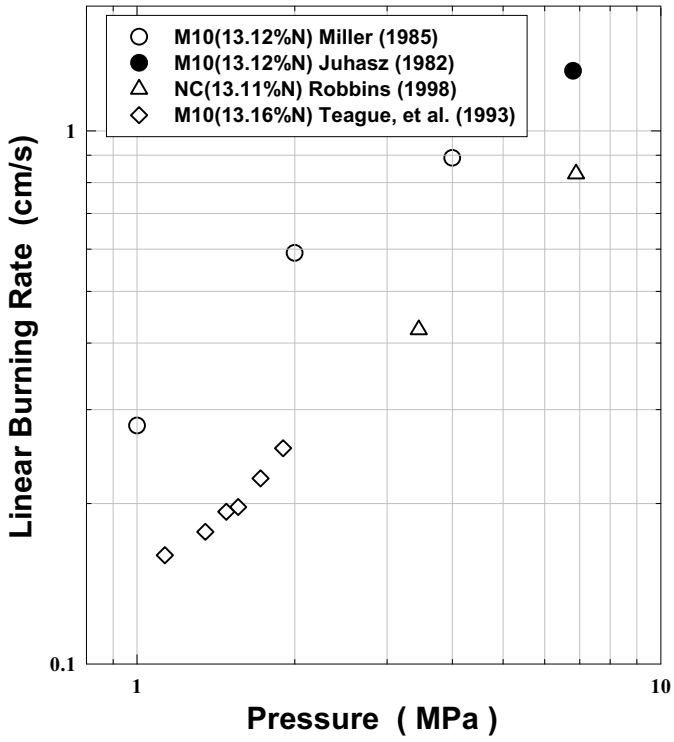

Figure 14. Burning rate of M10 vs. pressure. The pressurizing gas was N_2.

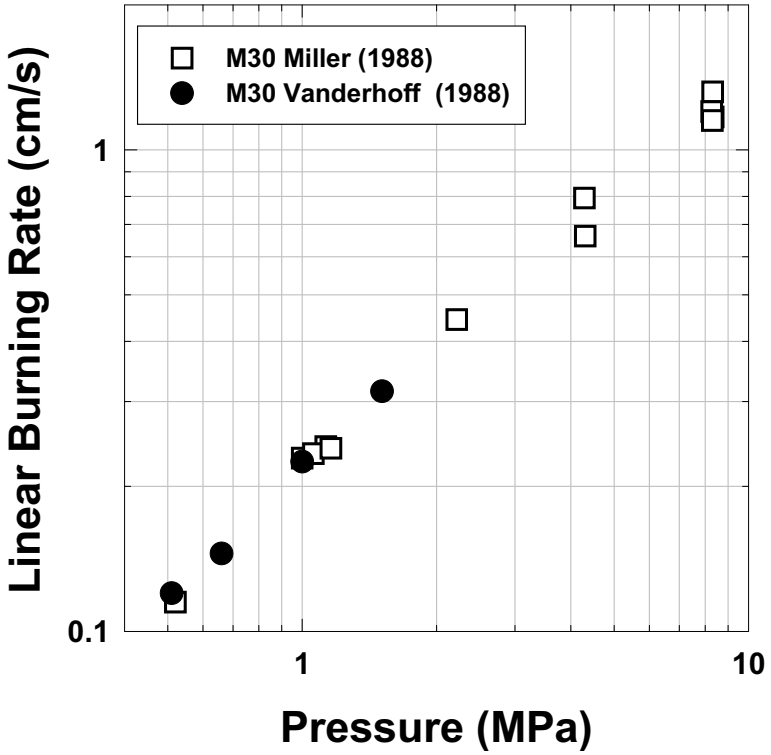

Figure 15. Burning rate of M30 vs.pressure. The pressurizing gas was N_2.

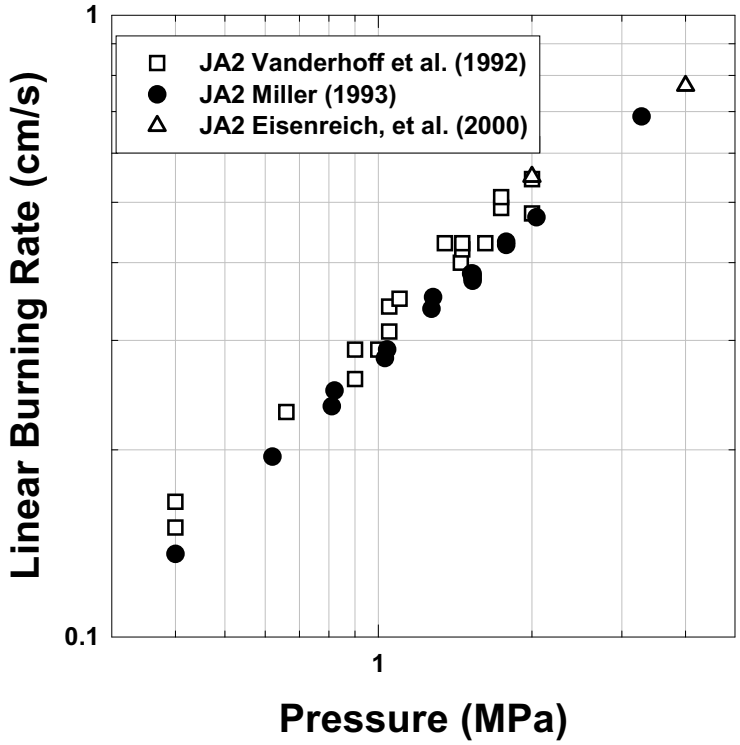

Figure 16. Burning rate of JA2 vs. pressure.

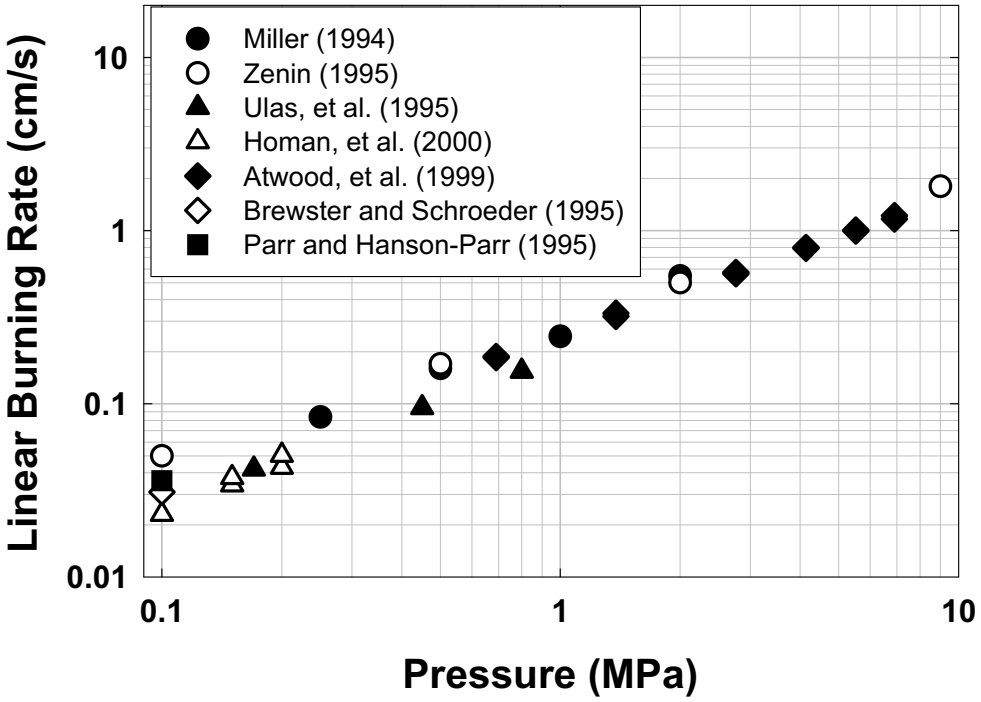

Figure 17. Burning rate of RDX as a function of pressure.

6. Appendix A

Table A-1. Some properties of the propellants shown in the video movies.

Propellant and Lot Number	Ingredients	Weight (%)	Diameter (cm)	Density (g/cm^3)	HOE[a] (cal/g)
HMX2	HMX (200/20 micron*)	80	0.6		780
	Polydiethylene Glycol Adipate	20			
JA2 RAD-PE-792-70	NC/13.04%N	58.21	1.3	1.58	1121
	Nitroglycerin	15.79			
	DEGDN	25.18			
	AKARDIT II	0.74			
	MgO	0.05			
	Graphite	0.03			
M10 RAD-PE-792-86	NC/13.16%N	97.73	1.3	1.53	895
	K_2SO_4	1.39			
	Diphenylamine	0.88			
M30 RAD-PE-792-83	NC/12.68%N	28.7	1.3	1.67	964
	Nitroglycerin	22.0			
	Nitroguanidine	47.3			
	Ethyl Centralite	1.6			
	Cryolite	0.4			
M43 IH-HELP1-09888-131-B3	RDX (5 micron*)	76	1.3	1.655	936
	Cellulose Acetate Butyrate	12			
	NC/12.6%N	4			
	Energetic Nitro Plasticizer	8			
RDX	RDX	100	0.8		
XM39 IH-XM39-0988-100-A3	RDX	76	1.3	1.636	830
	Cellulose Acetate Butyrate	12			
	NC/12.6%N	4			
	Acetyl Triethyl Citrate	7.6			
	Ethyl Centralite	0.4			

[a] The heat of explosion (HOE) has been copied from the propellant data sheets.

Table A-2. Burn rate data fitted to $r=Ap^n$, where r is the burn rate in cm/s and p is the pressure in MPa.

Propellant	A	n	Pressure Range - MPa
XM39 (Miller 1985)	.0488	0.92	1–4
XM39 (Teague 1993)	0.050	1.00	1–2
M43 (Kuo et al. 1993)	0.084	0.72	0.4–6
M43 (Teague et al. 1993)	0.070	1.41	1–2
M43 (Miller 1993)	0.085	0.82	0.4–8
HMX2 (Vanderhoff 1992)	0.048	1.08	1.2–2
HMX2 (Kubota 1982)	0.054	0.59	1–4
HMX2 (Edwards 1988)	0.057	0.77	1.8–3.5
M10 (Miller 1985)	0.035	0.68	1–4
M10 (Juhasz 1982)	0.173	0.80	3.5–7
M10 (Teague et al. 1993)	0.136	0.93	1.2–1.9
M30 (Miller 1988)	0.226	0.80	0.25–8.3
M30 (Vanderhoff 1988)	0.219	0.90	0.5–1.5
JA2 (Vanderhoff 1992)	0.312	0.81	0.4–2
JA2 (Miller 1993)	0.265	0.87	0.3–8.6
JA2 (Eisenreich 2000)	0.393	0.48	2–4
RDX (Miller 1994)	0.275	0.97	0.25–2
RDX (Zenin 1995)	0.284	0.84	0.1–9
RDX (Ulas 1995)	0.186	0.84	0.4–0.8
RDX (Homan 2000)	0.232	0.99	0.1–0.2
RDX (Atwood 1999)	0.250	0.81	0.7–10.3

7. References

Atwood, A. I., T. L., Boggs, P. O Curran, T. P. Parr, D. M. Hanson-Parr, C. F. Price, and J. Wiknich. "Burning Rate of Solid Propellant Ingredients, Part 1: Pressure and Initial Temperature Effects." *Journal of Propulsion and Power*, vol. 15, no. 6, pp. 740–747, 1999.

Brewster, M. Q., and T. B. Schroeder. "Experimental Study of Steady and Unsteady Combustion of RDX." *Proceedings of the 32nd JANNAF Combustion Meeting*, CPIA Publication 638, vol. 1, pp. 85–93, 1995.

Edwards, T. "Solid Propellant Flame Spectroscopy." AFAL-TR-88-076, Edwards Air Force Base, CA, 1988.

Eisenreich, N., W. Eckl, T. Fisher, V. Weiser, S. Kelzenberg, G. Langer, and A. Baier. "Burning Phenomena of the Gun Propellant JA2." *Propellants, Explosives, Pyrotechnics*, vol. 25, pp. 143–148, 2000.

Hatch, R. L. "Chemical Kinetics Combustion Model of the NG/Binder System." 24th JANNAF Combustion Subcommittee Meeting, CPIA Publication, no. 457, vol. 1, pp. 157–165, 1986.

Homan, B. E., and J. A. Vanderhoff. "Snapshot Absorption Spectroscopy." Applied Spectroscopy, vol. 53, pp. 816–821, 1999.

Homan, B. E., M. S. Miller, and J. A. Vanderhoff. "Absorption Diagnostics and Modeling Investigations of RDX Flame Structure." *Combustion and Flame*, vol. 120, pp. 301–317, 2000.

Juhasz, A. A. "Round Robin Results of the Closed Bomb and Strand Burner." CPIA Publication no. 361, pp. 1–15, 1982.

Kubota, N. "Physiochemical Processes of HMX Propellant Combustion." 19th Symposium (International) on Combustion, The Combustion Institute, p. 777, 1982.

Kuo, K. K., S. Thynell, P. Brown, T. Litzinger, V. Yang, and Y. Lu. "Ignition, Combustion and Kinetics of Energetic Materials." ARO-URI Contract No. DAAL03-92-G-0118, unpublished results, 1993.

Kuo, K. K., and Y. C. Ling. "Modeling of Physicochemical Processes of Burning RDX Monopropellants." Proceedings of the 20th International Pyrotechnics Seminar, pp. 583–600, 1994.

Maksimov, E. I., and A. G. Merzhanov. "On the Theory of Combustion of Condensed Materials." *Fiz. Goreniya Vzryva*, vol. 2, no. 1, pp. 46–58, 1966.

Miller, M. S., and W. R. Anderson. "Energetic-Material Combustion Modeling With Elementary Gas-Phase Reactions: A Practical Approach." *Solid Propellant Chemistry, Combustion, and Motor Interior Ballistics*, edited by V. Yang, T. B. Brill, and W. Z. Ren, vol. 185 of *Process in Aeronautics and Astronautics* (American Institute of Aeronautics and Astronautics, Reston, VA), chapter 2.12, 2000.

Miller, M. S. Unpublished data, U.S. Army Ballistic Research Laboratory, Aberdeen Proving Ground, MD, 1985.

Miller, M. S. Unpublished data, U.S. Army Ballistic Research Laboratory, Aberdeen Proving Ground, MD, 1988.

Miller, M. S. Unpublished data, U.S. Army Ballistic Research Laboratory, Aberdeen Proving Ground, MD, 1993.

Miller, M. S. Unpublished data, U.S. Army Ballistic Research Laboratory, Aberdeen Proving Ground, MD, 1994.

Parr, R. G., and B. L. Crawford, Jr. "A Physical Theory of Burning of Double-Base Rocket Propellants. I." *J. Phys. Chem.*, vol. 54, p. 929, 1950.

Parr, T., and D. Hanson-Parr. "RDX, HMX, and XM39 Self-Deflagration Flame Structure." 32nd JANNAF Combustion Subcommittee Meeting, CPIA Publication 631, vol. 1, pp. 429–437, 1995.

Rice, O. K., and R. Ginell. "The Theory of the Burning of Double-Base Rocket Powders." *J. Phys. Chem.*, vol. 54, p. 885, 1950.

Robbins, F. "Burning Rate-Flame Temperature Correlations for Pure NC Propellants." Advanced Solid CHON Propellant Burning Rate & Tailoring Workshop, CPIA Publication 677, p. 109, 1998.

Strehlow, R A. *Combustion Fundamentals*. McGraw-Hill Series in Energy, Combustion, and Environment, New York, p. 454, 1984.

Teague, M. Warfield, Singh, Gurbax and J. A. Vanderhoff. "Spectral Studies of Solid Propellant Combustion." ARL-TR-180, U.S. Army Research Laboratory, Aberdeen Proving Ground, MD, 1993.

Ulas, A., Y. C. Lu, K. K. Kuo, and T. Freyman. "Measurement of Temperatue and NO and OH Concentrations of Solid Propellant Flames Using Absorption Spectroscopy." *Proceedings of the 32nd JANNAF Combustion Meeting*, CPIA Publication 631, vol. 1, pp. 461–469, 1995.

Vanderhoff, J. A., M. Teague, Warfield, and A. J. Kotlar. "Absorption Spectroscopy Through the Dark Zone of Solid Propellant Flames." BRL-TR-3334, U.S. Army Ballistic Research Laboratory, Aberdeen Proving Ground, MD, 1992.

Vanderhoff, J. A. "Spectral Studies of Propellant Combustion: Experimental Details and Emission Results for M-30 Propellant." BRL-MR-3714, U.S. Army Ballistic Research Laboratory, Aberdeen Proving Ground, MD, 1988.

Zenin, A. "HMX and RDX: Combustion Mechanism and Influence on Modern Double-Base Propellant Combustion." *Journal of Propulsion and Power*, vol. 2, pp. 752–758, 1995.

Zimmer-Galler, R. "Correlations Between Deflagration Characteristics and Surface Properties of Nitramine-Based Propellants." *AIAA Journal*, vol. 6, no. 11, pp. 2107–2110, 1968.

NO. OF
COPIES ORGANIZATION

2 DEFENSE TECHNICAL
INFORMATION CENTER
DTIC OCA
8725 JOHN J KINGMAN RD
STE 0944
FT BELVOIR VA 22060-6218

1 HQDA
DAMO FDT
400 ARMY PENTAGON
WASHINGTON DC 20310-0460

1 OSD
OUSD(A&T)/ODDR&E(R)
DR R J TREW
3800 DEFENSE PENTAGON
WASHINGTON DC 20301-3800

1 COMMANDING GENERAL
US ARMY MATERIEL CMD
AMCRDA TF
5001 EISENHOWER AVE
ALEXANDRIA VA 22333-0001

1 INST FOR ADVNCD TCHNLGY
THE UNIV OF TEXAS AT AUSTIN
3925 W BRAKER LN STE 400
AUSTIN TX 78759-5316

1 DARPA
SPECIAL PROJECTS OFFICE
J CARLINI
3701 N FAIRFAX DR
ARLINGTON VA 22203-1714

1 US MILITARY ACADEMY
MATH SCI CTR EXCELLENCE
MADN MATH
MAJ HUBER
THAYER HALL
WEST POINT NY 10996-1786

1 DIRECTOR
US ARMY RESEARCH LAB
AMSRL D
DR D SMITH
2800 POWDER MILL RD
ADELPHI MD 20783-1197

NO. OF
COPIES ORGANIZATION

1 DIRECTOR
US ARMY RESEARCH LAB
AMSRL CI AI R
2800 POWDER MILL RD
ADELPHI MD 20783-1197

3 DIRECTOR
US ARMY RESEARCH LAB
AMSRL CI LL
2800 POWDER MILL RD
ADELPHI MD 20783-1197

3 DIRECTOR
US ARMY RESEARCH LAB
AMSRL CI IS T
2800 POWDER MILL RD
ADELPHI MD 20783-1197

ABERDEEN PROVING GROUND

2 DIR USARL
AMSRL CI LP (BLDG 305)

NO. OF
COPIES ORGANIZATION

ABERDEEN PROVING GROUND

31 DIR USARL
AMSRL WM BD
W R ANDERSON
R A BEYER
A BIRK
A L BRANT
S W BUNTE
C F CHABALOWSKI
L M CHANG
T P COFFEE
J COLBURN
P J CONROY
R A FIFER
B E FORCH
B E HOMAN
S L HOWARD
P J KASTE
A J KOTLAR
C LEVERITT
K L MCNESBY
M MCQUAID
M S MILLER
T C MINOR
A W MIZIOLEK
J B MORRIS
J A NEWBERRY
M J NUSCA
R A PESCE-RODRIGUEZ
G P REEVES
B M RICE
R C SAUSA
J A VANDERHOFF
A W WILLIAMS

REPORT DOCUMENTATION PAGE

Form Approved
OMB No. 0704-0188

1. AGENCY USE ONLY *(Leave blank)*	2. REPORT DATE	3. REPORT TYPE AND DATES COVERED
	July 2001	Final, October 1985–October 2000

4. TITLE AND SUBTITLE
Burning Phenomena of Solid Propellants

5. FUNDING NUMBERS
611102AH43

6. AUTHOR(S)
Martin S. Miller and John A. Vanderhoff

7. PERFORMING ORGANIZATION NAME(S) AND ADDRESS(ES)
U.S. Army Research Laboratory
ATTN: AMSRL-WM-BD
Aberdeen Proving Ground, MD 21005-5066

8. PERFORMING ORGANIZATION REPORT NUMBER
ARL-TR-2551

9. SPONSORING/MONITORING AGENCY NAMES(S) AND ADDRESS(ES)

10.SPONSORING/MONITORING AGENCY REPORT NUMBER

11. SUPPLEMENTARY NOTES

12a. DISTRIBUTION/AVAILABILITY STATEMENT
Approved for public release; distribution is unlimited.

12b. DISTRIBUTION CODE

13. ABSTRACT*(Maximum 200 words)*

Dynamic behavior of the burning surface of propellants has been captured as a function of pressure via movies taken with a 30-frames/s video camera. These movies can be played with the CD version of this manuscript. A windowed vessel capable of pressurization was used to burn the propellants XM39, M43, HMX2, M10, M30, JA2, and RDX over a pressure range from 0.1 to 3 MPa. The SVHS video camera was angled down to capture the dynamic surface behavior and provide some basis for assessing the validity of a one-dimensional approximation of the surface. Along with these propellant movies, plots of linear burning rate vs. pressure have been included.

14. SUBJECT TERMS	15. NUMBER OF PAGES
propellant burning, movies, burn rate, video frames, dynamic behavior	27
	16. PRICE CODE

17. SECURITY CLASSIFICATION OF REPORT	18. SECURITY CLASSIFICATION OF THIS PAGE	19. SECURITY CLASSIFICATION OF ABSTRACT	20. LIMITATION OF ABSTRACT
UNCLASSIFIED	UNCLASSIFIED	UNCLASSIFIED	unlimited UL